

Spectra of High-Redshift Type Ia Supernovae and a Comparison with their Low-Redshift Counterparts¹

I. M. Hook¹, D. A. Howell², G. Aldering³, R. Amanullah⁴, M. S. Burns⁵, A. Conley^{3,6}, S. E. Deustua⁷, R. Ellis⁸, S. Fabbro⁹, V. Fadeyev³, G. Folatelli⁴, G. Garavini^{4,10}, R. Gibbons¹¹, G. Goldhaber^{3,6}, A. Goobar⁴, D. E. Groom³, A. G. Kim³, R. A. Knop¹¹, M. Kowalski³, C. Lidman¹², S. Nobili^{4,10}, P. E. Nugent³, R. Pain¹⁰, C. R. Pennypacker³, S. Perlmutter^{3,6}, P. Ruiz-Lapuente¹³, G. Sainton¹⁰, B. E. Schaefer¹⁴, E. Smith¹¹, A. L. Spadafora³, V. Stanishev⁴, R. C. Thomas³, N. A. Walton¹⁵, L. Wang³, and W. M. Wood-Vasey^{3,6}
 (THE SUPERNOVA COSMOLOGY PROJECT)

ABSTRACT

We present spectra for 14 high-redshift ($0.17 < z < 0.83$) supernovae, which were discovered by the Supernova Cosmology Project as part of a campaign to measure cosmological parameters. The spectra are used to determine the redshift and classify the supernova type, essential information if the supernovae are to be used for cosmological studies. Redshifts were derived either from the spectrum of the host galaxy or from the spectrum of the supernova itself. We present evidence that these supernovae are of Type Ia by matching to spectra of nearby supernovae. We find that the dates of the spectra relative to maximum light determined from this fitting process are consistent with the dates determined from the photometric light curves, and moreover the spectral time-sequence for SNe Type Ia at low and high redshift is indistinguishable. We also show that the expansion velocities measured from blueshifted Ca H&K are consistent with those measured for low-redshift Type Ia supernovae. From these first-level quantitative comparisons we find no evidence for evolution in SNIa properties between these low- and high-redshift samples. Thus even though our samples may not be complete, we conclude that there is a population of SNe Ia at high redshift whose spectral properties match those at low redshift.

Subject headings: supernovae:general

¹Department of Physics, University of Oxford, Nuclear & Astrophysics Laboratory, Keble Road, Oxford, OX1 3RH, UK

²Department of Astronomy and Astrophysics, University of Toronto, 60 St. George St., Toronto, Ontario M5S 3H8, Canada

³E. O. Lawrence Berkeley National Laboratory, 1 Cyclotron Rd., Berkeley, CA 94720, USA

⁴Department of Physics, Stockholm University, AlbaNova University Center, S-106 91 Stockholm, Sweden

⁵Colorado College, 14 East Cache La Poudre St., Colorado Springs, CO 80903

⁶Department of Physics, University of California Berkeley, Berkeley, 94720-7300 CA, USA

⁷American Astronomical Society, 2000 Florida Ave,

NW, Suite 400, Washington, DC, 20009 USA.

⁸California Institute of Technology, E. California Blvd, Pasadena, CA 91125, USA

⁹CENTRA-Centro M. de Astrofísica and Department of Physics, IST, Lisbon, Portugal

¹⁰LPNHE, CNRS-IN2P3, University of Paris VI & VII, Paris, France

¹¹Department of Physics and Astronomy, Vanderbilt University, Nashville, TN 37240, USA

¹²European Southern Observatory, Alonso de Cordova 3107, Vitacura, Casilla 19001, Santiago 19, Chile

¹³Department of Astronomy, University of Barcelona, Barcelona, Spain

¹⁴Louisiana State University, Department of Physics and Astronomy, Baton Rouge, LA, 70803, USA

¹⁵Institute of Astronomy, Madingley Road, Cambridge

1. Introduction

The peak magnitudes of Type Ia supernovae (SNe Ia) are one of the best distance indicators at high redshifts, where few reliable distance indicators are available to study the cosmological parameters. Beginning with the discovery of SN 1992bi (Perlmutter et al. 1995), the Supernova Cosmology Project (SCP) has developed search techniques and rapid analysis methods that allow systematic discovery and follow up of “batches” of high-redshift supernovae. These searches and those of the High-z SN team have resulted in ~ 100 published SNe ($0.15 < z < 1.2$), which have been used for measurements of the cosmological parameters Ω_M and Ω_Λ and to provide initial constraints on the equation of state of the Universe, w (Perlmutter et al. 1998; Schmidt et al. 1998; Perlmutter et al. 1999; Garnavich et al. 1998; Riess et al. 1998; Knop et al. 2003; Barris et al. 2004; Tonry et al. 2003; Riess et al. 2004).

Spectra have been obtained for as many of the SCP supernovae as possible, and as close as possible to maximum light. The spectra are used to determine the redshift of the event and to confirm its spectral sub-type, both crucial if the supernova is to be used in a determination of cosmological parameters. In addition the spectra provide a check that SNe Ia at high redshift are similar to those at low redshift, an assumption central to the use of SNe Ia as ‘standardized candles’. This paper represents a significant contribution to the amount of published high-redshift SN Ia spectroscopy (Lidman et al. 2005; Barris et al. 2004; Tonry et al. 2003; Coil et al. 2000; Matheson et al. 2005).

In this paper we present spectra for a subset of our distant supernovae, discovered during search campaigns in January and March 1997. Since the goal of this paper is a first quantitative comparison of high- and low-redshift SN spectra, spectra were chosen where the SN features were relatively

CB3 0HA, UK

¹Much of the data presented herein were obtained at the W.M. Keck Observatory, which is operated as a scientific partnership among the California Institute of Technology, the University of California and the National Aeronautics and Space Administration. The Observatory was made possible by the generous financial support of the W.M. Keck Foundation. Also based in part on observations made with the European Southern Observatory telescopes (ESO programs 58.A-0745 and 59.A-0745).

clear. Spectra of 33 objects were taken during the two campaigns, of which four were found to be clear broad-lined QSOs and two were “featureless” blue objects (possibly BL Lacs) for which a redshift could not be measured. The other objects all have measured redshifts and of these about half (13) were rejected for the purposes of this paper based on one or both of the following criteria: low signal-to-noise ratio (i.e. less than about 10 per 20Å bin over the observed wavelength range 6000–8000Å) or large contamination by the host galaxy, roughly corresponding to a percentage increase of less than 50% in R -band photometry between reference and “new” images (although the latter is only a rough guide since the phase of the SN, its location relative to the core of the galaxy and the seeing all strongly affect how clearly the SN appears in the spectrum).

The spectra presented here provide the basis for the identification of these objects as Type Ia, as quoted in Perlmutter et al. (1999) and Knop et al. (2003). Future papers by G. Garavini et al. and E. Smith et al. will present spectroscopic results and analysis on other SCP datasets.

For each object in our sample we give the redshift and present the results of matching the spectrum to various supernova templates (including SNe of Types other than Ia), and hence give spectroscopic evidence that these distant supernovae are of Type Ia. The spectral dates derived from this matching process are compared with the dates derived from the light curves. Finally we present the set of high-redshift SN spectra as a time sequence showing that the spectrum changes with light curve phase in a similar way at low and high redshift.

2. Discovery of the Supernovae

The observing strategy developed for these high-redshift SN search runs involved comparison of large numbers of galaxies in each of ~ 50 $14.7' \times 14.7'$ fields observed twice with a separation of 3–4 weeks (Perlmutter et al. 1997). This strategy ensures that almost all the supernovae are discovered before maximum light, and, since it could be guaranteed that at least a dozen supernovae would be found on a given search run, the follow-up observing time could be scheduled in advance. This strategy made it possible to sched-

ule spectroscopy time on large telescopes while the supernovae were still close to maximum light, and thus the supernova features can be observed even at redshifts >1 . Follow-up photometric measurements were also made of the supernova light-curves, from which the maximum brightness and date of maximum is derived.

The supernovae described in this paper were identified on R -band images taken in two searches on the CTIO 4-m Blanco telescope in January and March 1997. Candidate supernovae were identified on the difference images (see Perlmutter et al. (1997) for details on the identification of candidates). Those supernovae identified as Type Ia were followed photometrically in the R - and I -bands at the WIYN telescope at KPNO, the ESO 3.6m and one (SN 1997ap) was followed with the *Hubble Space Telescope* (Perlmutter et al. 1998).

Parameterised light-curve fits for all but one of the objects presented in this paper (SN 1997ag, which does not have sufficient photometric light curve measurements for cosmological use) are published in Perlmutter et al. (1999). These SNe form part of the set that provided the first evidence for the accelerating expansion of the universe and the presence of some form of dark energy driving this expansion. Many of these objects (but excluding SN 1997ag, SN 1997G, SN 1997J and SN 1997S because of poor colour measurements, $\sigma_{R-I} > 0.25$) were also used in the more recent measurements of cosmological parameters by Knop et al. (2003).

3. Spectroscopic Observations

The spectra were obtained during two observing runs at the Keck-II 10-m telescope (two nights in January and three in March 1997) and one run at the ESO 3.6m (1 night in January 1997). The spectroscopic runs were scheduled to occur within one week of the corresponding search run at CTIO. At the time of observations, close to maximum light, the typical magnitudes of the supernova candidates were 22-24 magnitude in R -band and in many cases their host galaxies had similar apparent magnitudes. In all cases where the galaxy was bright enough, the slit was aligned at a position angle on the sky such that the supernova and the center of the host galaxy were both in the slit. This was done to allow redshift determination from features in the host galaxy spectrum.

Observations of the spectrophotometric standards HD84937, HD19445 and BD262606 (Oke & Gunn 1983) were taken at Keck-II, and LTT 1788 (Stone & Baldwin 1983; Baldwin & Stone 1984; Hamuy 1994) was observed at ESO, in order to obtain approximate relative flux calibration of the spectra. The standards were observed at the parallactic angle, although note that the SN spectra were not necessarily taken at the parallactic angle as described above. Although the effects of atmospheric dispersion are small when observing in the red (as is the case for these spectra), some small wavelength-dependent slit losses may occur. Therefore the overall slope of the spectra is not considered to be reliable and the slope is left as a free parameter in the analysis that follows.

Keck data The LRIS spectrograph (Oke et al. 1995) with the 300 l/mm grating was used at the Cassegrain focus of the Keck-II 10m telescope. The spectra cover the wavelength range 5000 to 10000Å with dispersion of $\sim 2.5\text{\AA}$ per pixel. Typical exposure times were 0.5 to 1.5 hours.

During the January run, dome flats were taken at the position of targets when possible. This was necessary because flexure causes the fringe pattern to shift depending on the zenith distance and rotator angle. Previous tests showed that dome flats gave marginally better results compared to internal flats when trying to subtract sky lines at the red end of the spectrum. During the March run, bad weather and technical problems severely limited the amount of usable time. Therefore, to allow us to observe all the candidates, the exposure times for each object were reduced and only internal flats were taken. Hg-Ne-Ar arc spectra for wavelength calibration were obtained at the same position as the flats.

ESO 3.6m data The EFOSC1 spectrograph (Buzzoni et al. 2004) was used at the cassegrain focus of the ESO 3.6m. The R300 grism was used, giving a dispersion of 3.5Å/pixel over the range 5900 to 10000Å. Dome flats were used to flat-field the data, and wavelength calibration was carried out using observations of He-Ar (ESO) arc lamps.

Table 1 gives the dates and exposure times for the observations of the various supernova candidates.

TABLE 1
SUMMARY OF SPECTRAL OBSERVATIONS.

IAU name	R mag ^a	Telescope	Exp (hours)	Date (UT)
1997F	23.9	Keck-II	1.0	1997 Jan 12
1997G	23.7	Keck-II	1.3	1997 Jan 13
1997I	20.9	ESO 3.6m	1.0	1997 Jan 13
1997J	23.4	Keck-II	1.3	1997 Jan 13
1997N	21.0	ESO 3.6m	0.5	1997 Jan 13
1997R	24.4	Keck-II	1.4	1997 Jan 13
1997S	23.6	Keck-II	1.8	1997 Jan 13
1997ac	23.1	Keck-II	0.17	1997 Mar 14
1997af	23.8	Keck-II	0.58	1997 Mar 14
1997ag	23.2	Keck-II	0.25	1997 Mar 14
1997ai	22.3	Keck-II	0.35	1997 Mar 13
1997aj	22.3	Keck-II	0.67	1997 Mar 13
1997am	22.9	Keck-II	0.31	1997 Mar 13
1997ap	24.2	Keck-II	1.5	1997 Mar 14

^aThe magnitudes given are for the supernovae at the time of the spectroscopic observations, and were estimated from nearby light-curve photometry points. These are accurate to about 0.2 mag.

4. Data Reduction

The spectra were reduced using the IRAF² spectral reduction package. The data were first overscan-subtracted, bias corrected and flat-fielded using the flats described above. The spectra were then extracted to provide 1-D spectra of the targets. In some cases the supernova was sufficiently offset from the core of its host galaxy that it was possible to extract the supernova spectrum and that of the host galaxy separately. In other cases it was only possible to extract a single spectrum containing a mix of supernova and host galaxy light. These spectra were then wavelength calibrated and flux calibrated. Except where otherwise stated explicitly, a correction for atmospheric absorption features was made.

5. Identification

SNe Ia are classified spectroscopically by a lack of hydrogen and the presence of a strong Si II feature at $\sim 6150\text{\AA}$ in the rest frame (see Filippenko (1997) for a review). However, at redshifts above 0.5 this line moves into the infrared and can no longer be seen with typical CCDs. Therefore we use the following criteria to classify a spectrum as a SN Ia when this line is not seen:

- Presence of the SII “W” feature at $\sim 5500\text{\AA}$. This is only seen in Type Ia supernovae (see Figure 1).
- Presence of Si II feature at $\sim 4000\text{\AA}$. If seen, this feature indicates that the supernova is definitely of Type Ia, although for spectra prior to maximum light or for SN 1991T-like SNe Ia, this feature can be weak. Note that it is easy to mistake Ca H&K from the host galaxy for this feature.
- The combination of both the light curve age with the temporal evolution of the Fe II features at ~ 4500 and 5100\AA . In a SN Ib/c at maximum light, these Fe II features resemble those in a SN Ia about two weeks after maximum light (Figure 1), but the appearance

²IRAF is distributed by the National Optical Astronomy Observatories, which are operated by the Association of Universities for Research in Astronomy, Inc., under cooperative agreement with the National Science Foundation.

of a Type Ia spectrum at maximum light is unique.

5.1. Matching Technique

The spectra in this paper were matched against template SN spectra using a spectrum matching code developed by Howell & Wang (2002). All fits were performed after rebinning the data to 20\AA to allow more rapid runs of the fitting program. At a given redshift, the code computes:

$$\chi^2 = \frac{w(\lambda)(O(\lambda) - aT(\lambda)10^{cA_\lambda} - bG(\lambda))^2}{\sigma(\lambda)^2},$$

where $w(\lambda)$ is a weighting function, O is the observed spectrum, T is the SN template spectrum, G is the host galaxy template spectrum, A_λ is the reddening law, σ is the error on the spectrum, and a , b , and c are constants that are varied to find the best fit. The weighting function was set to be unity across the spectrum except at the telluric features, which were given zero weight. This equation is iterated over a range of redshifts to find the minimum χ^2 in redshift, host galaxy, template supernova, and reddening space. In this analysis, the reddening law (Cardelli et al. (1989); O’Donnell (1994)) was fixed at $R_V = 3.1$, although the spectrum matching code can handle other values of R_V .

When the redshift was well determined from narrow galaxy lines, it was constrained in the fits. Likewise, when the host galaxy type was known from Sullivan et al. (2003), it was fixed in the following manner. For Sullivan type 0, E and S0 galaxies were tested. For type 1, Sa and Sb galaxies were allowed, and for type 2, Sb, Sc, and starburst galaxy types were used. The galaxy templates subtracted here were those of Kinney et al. (1993) which have been smoothed and had their narrow lines removed.

In three cases, SN 1997ac, SN 1997ai and SN 1997ap, it was not possible to obtain a host galaxy redshift. In these cases the redshift was determined from fits to SN templates. For each template, the best-fit redshift was determined by stepping through redshift space in 0.001 increments. In section 5.3 we describe the estimation of redshift uncertainties for these cases.

The fitting program is intended to aid human classifiers of SN spectra — it is not a replacement

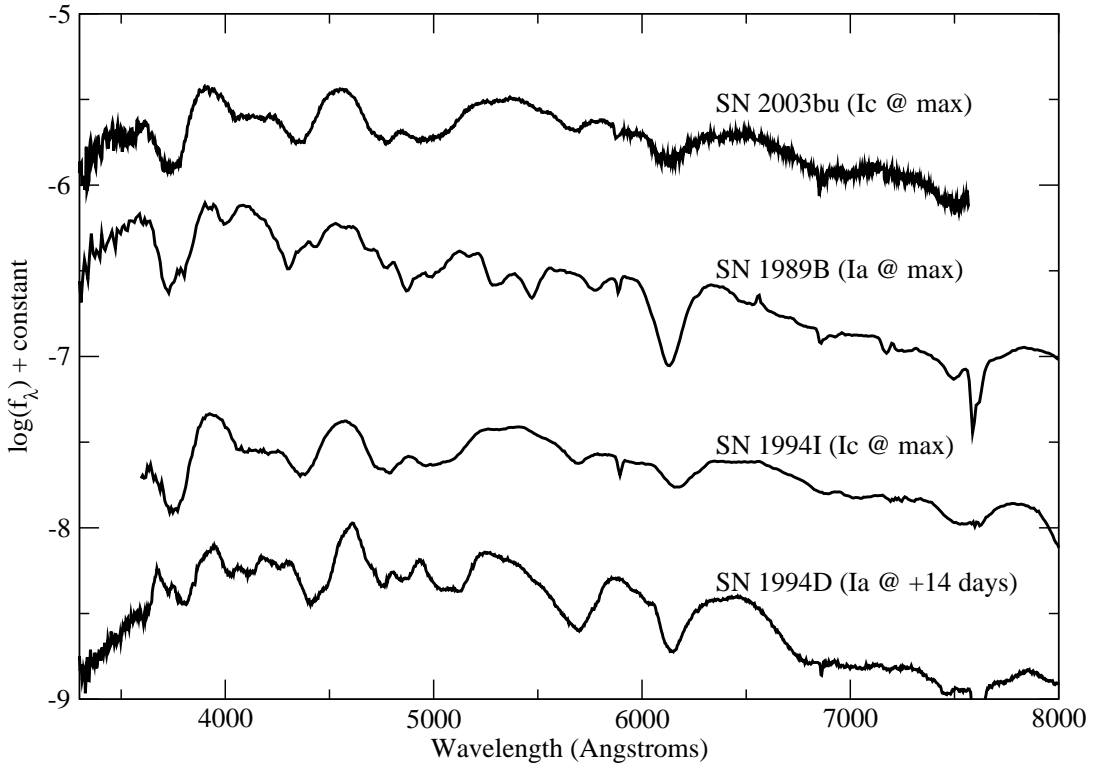


Fig. 1.— Comparison of nearby SNe Ia and Ic at maximum light. SNe Ic can closely resemble SNe Ia blueward of 4500Å with the exception of the 4000Å Si II feature. Also, SNe Ic have a group of Fe features spanning 4500–5200Å that resemble the same features in a Type Ia spectrum ~ 2 weeks after maximum light. The data shown are SN 1989B (Wells et al. 1994), SN 2003bu (P. Nugent, private communication), SN 1994I (Clocchiatti et al. 1996) and SN 1994D (Meikle et al. 1996).

for them. The program returns a list of fits in decreasing order of goodness-of-fit. The output is inspected and a “best fit” is chosen. A good indication of the level of certainty of a match is the amount of agreement between the best fits. For data with good signal-to-noise ratio (S/N) and little host contamination, there is almost always excellent agreement between the top five fits.

The program is also limited by the available template data. For example, less than a dozen SNe have UV spectroscopy near or before maximum light (Cappellaro et al. 1995), and core collapse SNe are particularly underrepresented in terms of UV observations. Thus at high redshift, where the observed optical band corresponds to rest-frame UV, it can be hard to obtain conclusive results. One other problem area is at very early times. From day -18 to -8 there are few spectra of SNe Ia, and these are the epochs where SNe Ia show the greatest diversity. Furthermore, Si II 4000Å can be weak or absent at very early times, making a secure classification difficult. Finally, a week after maximum light SNe Ib/c and SNe Ia show the greatest similarity in their spectra (see Figure 1). We note that more UV spectra of SNe Ib/c would be beneficial to the classification process. With such spectra it would be possible to confirm some cases which are probable Type Ia but for which Type Ib/c cannot be eliminated. If Si II 6150Å is not in the observed spectral range, or there is host contamination, classification at this phase can be harder than at other phases. The list of nearby supernovae used in the fitting process is given in Table 2. A full list of the dates of these spectra and their references will be presented by Howell (in preparation).

Near maximum light, normal SNe Ia show a characteristic pattern of absorption features at rest-frame 3800Å (Ca II), 4000Å (Si II), 4300Å (Mg II and Iron-peak lines), 4900Å (various Iron-peak lines), 5400Å (SII ‘W’), 5800Å (Si II and Ti II), and 6150Å (Si II). If the S/N of the spectrum is low, typical Ia-indicator lines such as Si II and SII may be hard to identify definitively. However, the overall pattern of features in a SN Ia at a given epoch is unique, so fits to the overall spectrum (with sufficient S/N) can allow a secure classification of the SN type, especially when there is an independent confirmation of the SN epoch from the light curve.

In summary, this procedure provides a more robust measure of the SN type than unaided human typing by eye. Furthermore, it uses the shape of the entire spectrum to classify SNe, not just one or two key features. The technique also provides a spectroscopic determination of the rest-frame date the spectrum was taken (relative to maximum light), which can be checked against the light curve, yielding an independent consistency check as shown in the next section.

5.2. Matching Results

The results of the fitting procedure are given in Table 3. We show the best fit SN template, the type of host galaxy that was subtracted (if any), the redshift, and the epoch of the template spectrum. In addition, we give a “spectroscopic epoch,” which is the weighted average of the epochs from the five best-fit spectra. This spectroscopic determination of the epoch of the SN can be compared with the epoch determined from the light curve, also presented in Table 3. Figure 2 shows that the two numbers are in good agreement, with an RMS difference of 3.3 days.

The program also formally returns an estimate of the amount of reddening (or de-reddening) required to match the observed spectrum, but this number may not reflect the actual reddening toward the SN. This parameter accounts for all differences in color between the observation and the template, so differential slit losses due to observations not taken at the parallactic angle, wavelength-dependent seeing, errors in flux calibration, and uncorrected reddening in the templates, all make an accurate determination of the reddening to the SN from this spectroscopy alone unfeasible.

5.3. Measurement of redshifts

In most cases the slit angle for the spectroscopic observations was chosen so that light from both the SN and the host galaxy (when visible on the CTIO images) fell down the slit. Since features in the galaxy spectra are typically much narrower than those in supernova spectra it is often possible to obtain a redshift from the galaxy features, even in cases where the supernova and host galaxy light are blended. Table 3 summarises the measured redshifts.

TABLE 2

A LIST OF THE NEARBY SUPERNOVAE USED AS TEMPLATES IN THE FITTING PROCEDURE. DETAILS OF THE DATES OF THESE SPECTRA AND THEIR REFERENCES WILL BE PRESENTED BY HOWELL (IN PREPARATION). THE SUSPECT SN ARCHIVE (RICHARDSON ET AL. 2002) WAS USED IN THE CREATION OF THIS LIBRARY.

SN Type	Supernova Name
Ia	SN 1981B, SN 1986G, SN 1989B, SN 1990N, SN 1991T, SN 1991bg, SN 1992A, SN 1994D, SN 1996X, SN 1998bu, SN 1999aa, SN 1999ac, SN 1999ao, SN 1999av, SN 1999aw, SN 1999be, SN 1999bk, SN 1999bm, SN 1999bn, SN 1999bp, SN 1999ee
II	SN 1979C, SN 1980K, SN 1984E, SN 1986I, SN 1987A, SN 1987B, SN 1987K, SN 1988A, SN 1988Z, SN 1993J, SN 1993W, SN 1997cy, SN 1999em, SN 1999em ^a
Ibc	SN 1983N, SN 1983V, SN 1984L, SN 1987M, SN 1988L, SN 1990B, SN 1990U, SN 1990aa, SN 1991A, SN 1991K, SN 1991L, SN 1991N, SN 1991ar, SN 1994I, SN 1995F, SN 1995bb, SN 1996cb, SN 1997C, SN 1997dd, SN 1997dq, SN 1997ei, SN 1997ef, SN 1998bw, SN 1998dt, SN 1999P, SN 1999bv, SN 1999di, SN 1999dn, SN 1999ex, SN 2000H

^aTheoretical SN 1999em spectra provided by Peter Nugent

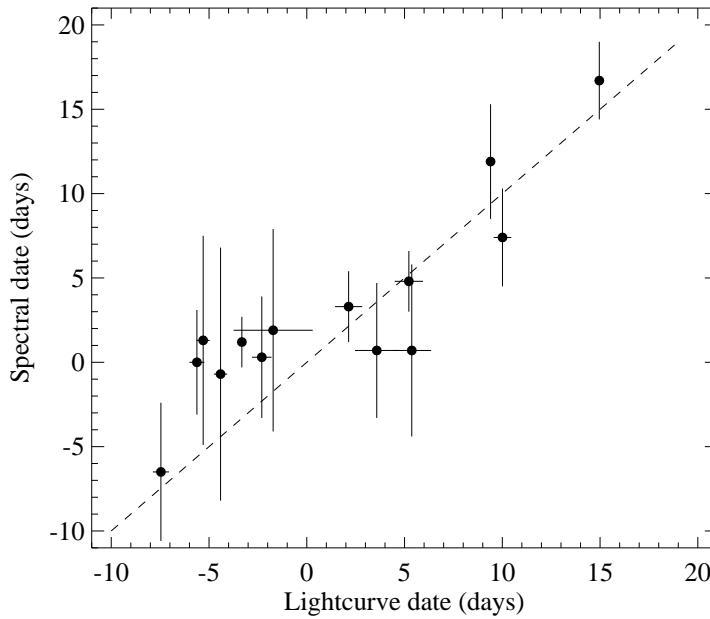


Fig. 2.— Comparison of the epoch of the spectrum as determined from the light curve (τ_{lc}) with that determined from the weighted average of the 5 best template fits to the spectrum (τ_s). In both cases the epochs are expressed as rest-frame days relative to maximum light. The dashed line shows the locus $\tau_{lc} = \tau_s$.

TABLE 3
SUMMARY OF FITTING RESULTS.

IAU name	z	τ_{lc}^a	τ_s^b	τ_t^c	Match	G^d	G^e
1997F	0.580 ± 0.001	-7.5 ± 0.4	-6.5 ± 4.1	-8	1999ee	1	Sa
1997G	0.763 ± 0.001	$+5.4 \pm 1.0$	$+0.7 \pm 5.1$	$+4$	1999bk	2	-
1997I	0.172 ± 0.001	-3.3 ± 0.1	$+1.2 \pm 1.5$	$+1$	1999bp	1	Sb
1997J	0.619 ± 0.001	$+3.6 \pm 1.1$	$+0.7 \pm 4.0$	$+2$	1999bn	0	S0
1997N	0.180 ± 0.001	$+15.0 \pm 0.1$	$+16.7 \pm 2.3$	$+15$	1991T	2	SB2
1997R	0.657 ± 0.001	-5.6 ± 0.4	$+0.0 \pm 3.1$	-5	1989B	1	Sa
1997S	0.612 ± 0.001	$+2.1 \pm 0.7$	$+3.3 \pm 2.1$	$+5$	1992A	-	SB1
1997ac	0.323 ± 0.005^f	$+9.4 \pm 0.1$	$+11.9 \pm 3.4$	$+11$	1998bu	-	-
1997af	0.579 ± 0.001	-5.3 ± 0.3	$+1.3 \pm 6.2$	-2	1999bp	2	SB6
1997ag	0.592 ± 0.001	-1.7 ± 2.0^g	$+1.9 \pm 6.0$	-7	1990N	-	Sa
1997ai	0.454 ± 0.006^f	$+5.2 \pm 0.7$	$+4.8 \pm 1.8$	$+5$	1992A	-	-
1997aj	0.581 ± 0.001	-4.4 ± 0.3	-0.7 ± 7.5	-3	1999aa	2	Sb
1997am	0.416 ± 0.001	$+10.0 \pm 0.5$	$+7.4 \pm 2.9$	$+9$	1992A	2	SB1
1997ap	0.831 ± 0.007^f	-2.3 ± 0.5	$+0.3 \pm 3.6$	-5	1989B	2	-

The uncertainties in these redshifts were estimated as described in section 5.3.

^aSpectral epoch relative to B light curve maximum (in the rest frame) as determined from light curve fitting (Knop et al. 2003)

^bSpectral epoch from weighted average of 5 best-fit spectra. The uncertainty quoted is the weighted standard deviation of the epochs of the 5 best SN Ia fits.

^cSpectral epoch of best matching comparison template spectrum.

^dHost galaxy type from Sullivan et al. (2003); 0: E-S0, 1: Sa-Sb, 2: Sc and later

^eTemplate host galaxy spectrum subtracted from the data for the fits.

^fRedshift determined from the supernova alone. These values are derived based on the matching procedure described in section 5.1 and supercede those in Perlmutter et al. (1999); Knop et al. (2003).

^gThis SN has a poorly-constrained light-curve because only a small number of photometric measurements were made. In order to estimate the time of maximum it was necessary to constrain the stretch parameter to $s=1$ when fitting the light-curve.

In the cases where galaxy features were visible, the centroids of the lines were measured, and the redshift calculated by taking the mean of the redshifts derived from the individual lines. The uncertainty in the mean redshift z is estimated as ± 0.001 .

In the cases where there were no identifiable host galaxy features to determine the redshift (SN 1997ac, SN 1997ai and SN 1997ap), the redshift was determined from fits to SN templates as described in section 5.1. In order to estimate the uncertainty in these redshifts we used the other 11 cases, whose redshifts were known from the host galaxies, as follows. Each high-redshift spectrum was cross-correlated with the corresponding best-fit template (using the IRAF cross-correlation routine “*fxcor*”) allowing redshift to vary. In this sample of 11 cases, we found a mean redshift difference between SN and host redshift of -0.0012 and an RMS difference of 0.005. Thus there does not appear to be any significant systematic redshift error and the uncertainty in redshift is about 0.005. This test measures the uncertainty in redshift determination when the “correct” template is used. For cases where the redshift is not known from the host galaxy there is an additional uncertainty from the diversity of velocities seen in nearby template spectra. To estimate the size of this effect we took the standard deviation of the velocity of the Si II 6150Å feature for the SNe Ia presented in Benetti et al. (2005). Our calculated value of 1300 km s^{-1} corresponds to a redshift uncertainty of 0.004. Combining these two effects in quadrature gives an estimated uncertainty in redshift of about 0.006 on average. However we also note the uncertainties should increase with redshift (and indeed this general trend is seen in our sample of 11 objects) because the lines become broader, the S/N becomes poorer, and the spectrum corresponds more to the rest-frame UV where there are fewer templates available. Thus we use a simple relation of $0.004 \times (1 + z)$ to estimate the errors (which gives an error of 0.006 at our average redshift of $z \sim 0.5$).

6. Results

Figures 3 to 16 show the spectra, all in F_λ units with arbitrary normalisation. The top panel shows the unsmoothed spectrum which typically

contains both supernova and galaxy light. In the cases where the supernova and galaxy light were resolved and separate extractions were possible, the top panel shows the unsmoothed data for the host galaxy. The lower panels show the results of the template matching described in the previous section. In almost all cases clear supernova Ia features are visible in the high-redshift supernova spectrum.

6.1. Notes on Individual Objects

SN 1997F (Figure 3). This spectrum is a blend of galaxy and SN light (the host galaxy and SN were not separable in the extraction). The host galaxy has $z = 0.580 \pm 0.001$, based on narrow lines from [OII], H γ , G-band and [OIII]. After subtraction of a galaxy template, broad Ca II is visible. In a SN Ia at this epoch (-7 days), other features are weak, so it is difficult to distinguish them given the S/N of this spectrum. Though the spectrum is dominated by galaxy light, two lines of evidence give us confidence that the residual spectrum is a Type Ia SN. Firstly, the epoch determined by the fitting program (-6.5 days) agrees well with the epoch determined from the light curve (-7.5 days). Secondly, a Type Ia is a much better fit to the data than any other SN Type.

SN 1997G (Figure 4). The supernova is slightly merged with a brighter galaxy which has $z = 0.763 \pm 0.001$. SN Ia features can be seen at the same redshift. The fact that the two objects were merged together made sky subtraction difficult, and residuals remain at observed wavelengths $\lambda_{obs} = 5577\text{\AA}$ and 6300\AA . These have been interpolated across for the Figures. While we consider a Type Ia identification to be the most probable for this SN, a Type Ib/c identification cannot be ruled out due to the lack of definitive Si II and the poor S/N redward of $\sim 8200\text{\AA}$, corresponding to $\sim 4650\text{\AA}$ in the rest frame. Furthermore, there are few UV spectra of SNe Ib/c, so while the bumps at 2900\AA and 3150\AA (rest frame) observed at $\sim 5110\text{\AA}$ and $\sim 5550\text{\AA}$ match those in a Ia, the behaviour of SNe Ib/c in this region is not well studied.

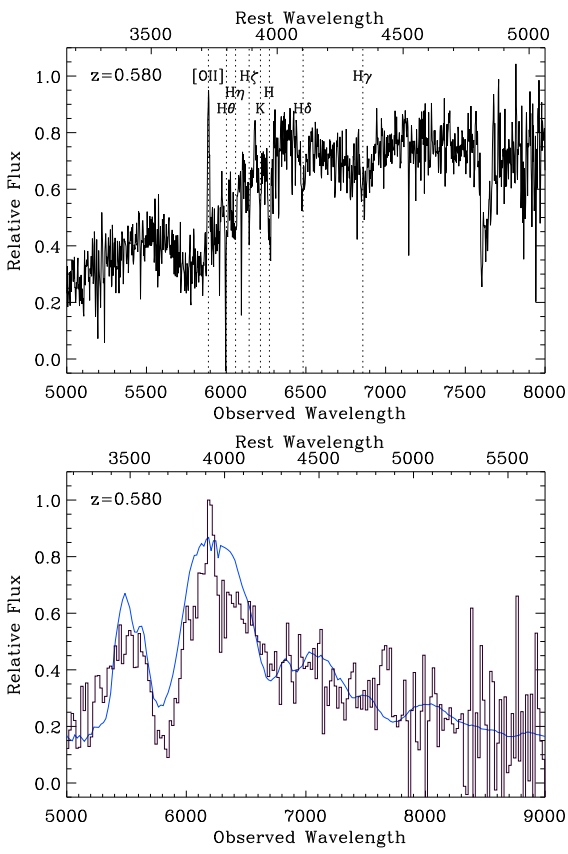


Fig. 3.— (Upper) Unsmoothed spectrum of SN 1997F showing narrow features used to determine the redshift (note that atmospheric absorption has not been corrected in this spectrum). (Lower) Re-binned spectrum of SN 1997F (histogram) after interpolating over narrow galaxy lines and sky absorption feature at 7600Å, and subtracting template Sa galaxy, compared with SN 1999ee at –8 days (smooth curve).

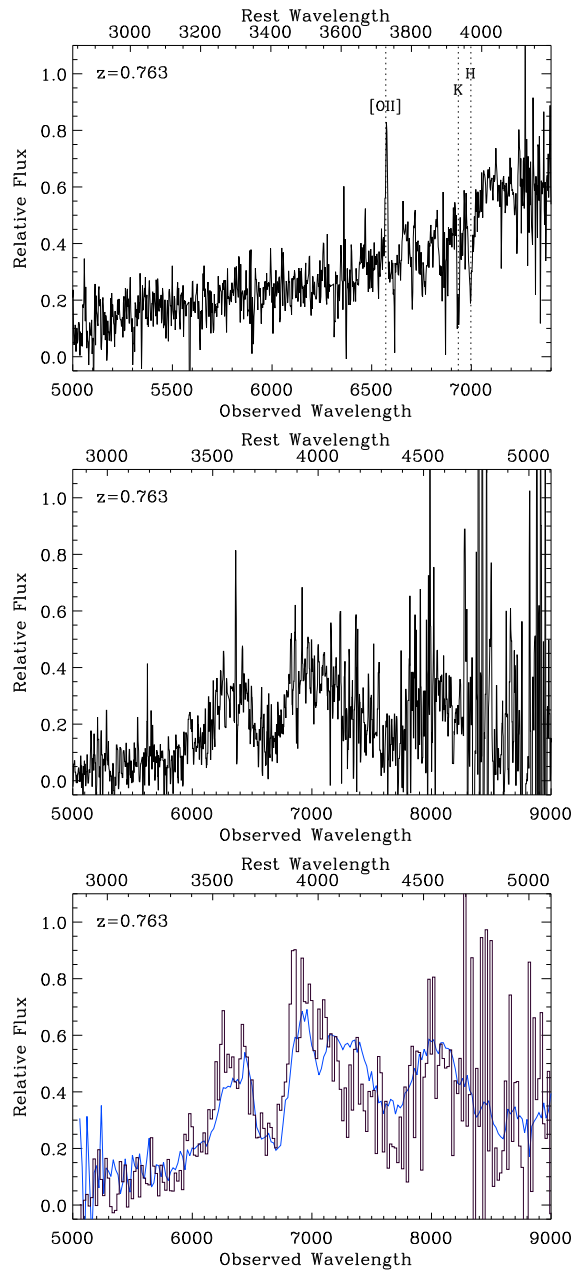


Fig. 4.— (Upper) Lightly smoothed spectrum of neighbouring (host) galaxy of SN 1997G (note that atmospheric absorption has not been corrected in this spectrum). (Lower) Lightly smoothed spectrum of the supernova SN 1997G (lower) re-binned spectrum of SN 1997G (histogram) after interpolating over poorly-subtracted sky lines and subtracting an Sa galaxy template, compared with SN 1999bk at +4 days (smooth curve).

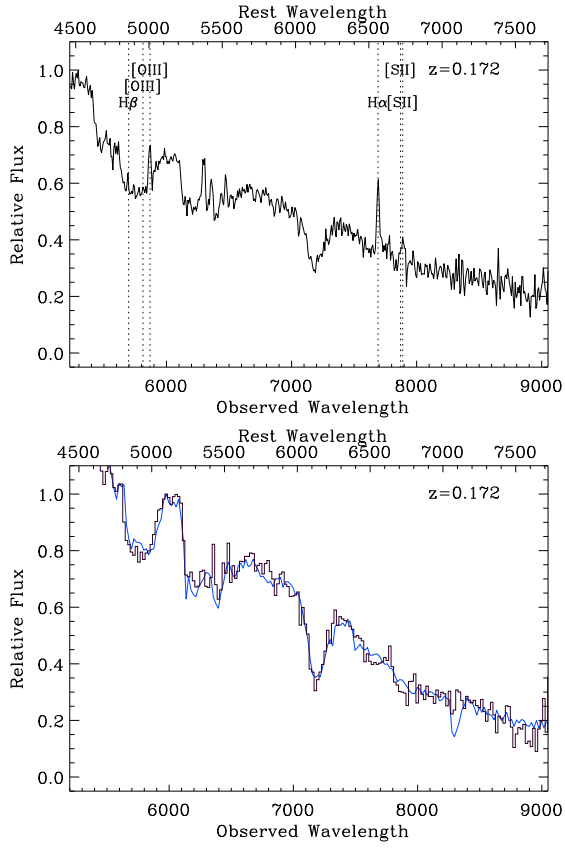


Fig. 5.— (Upper) Unsmoothed spectrum of SN 1997I obtained at the ESO 3.6m showing galaxy lines used to determine the redshift. (Lower) Re-binned spectrum of SN 1997I (histogram) after interpolating over narrow galaxy lines and subtraction of an Sb template galaxy spectrum, compared with SN 1999bp at +1 day (smooth curve).

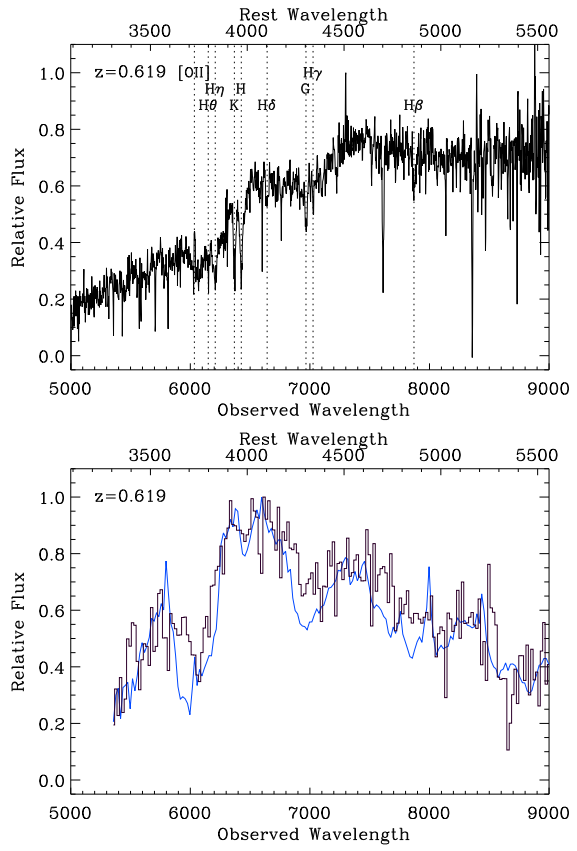


Fig. 6.— (Upper) Unsmoothed spectrum of SN 1997J showing the narrow lines used to determine the redshift. (Lower) rebinned spectrum of SN 1997J (histogram) after subtraction of template S0 host galaxy, compared with SN 1999bn at day +2 (smooth curve).

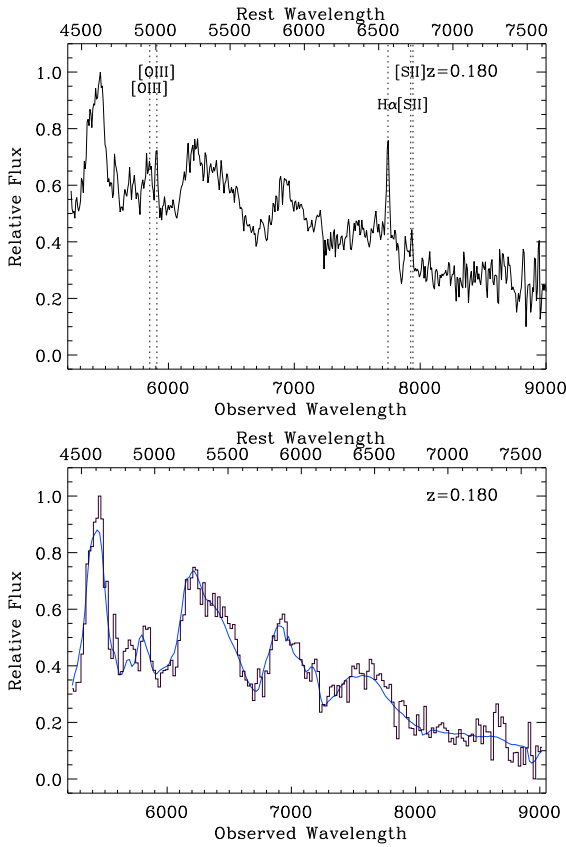


Fig. 7.— (Upper) Unsmoothed spectrum of SN 1997N showing the narrow lines used to determine the redshift. (Lower) Rebinning spectrum of SN 1997N (histogram) after interpolating over strong emission lines of [OIII] and H α and subtracting template SB2 host galaxy light, compared with SN 1991T at +15 days (smooth curve).

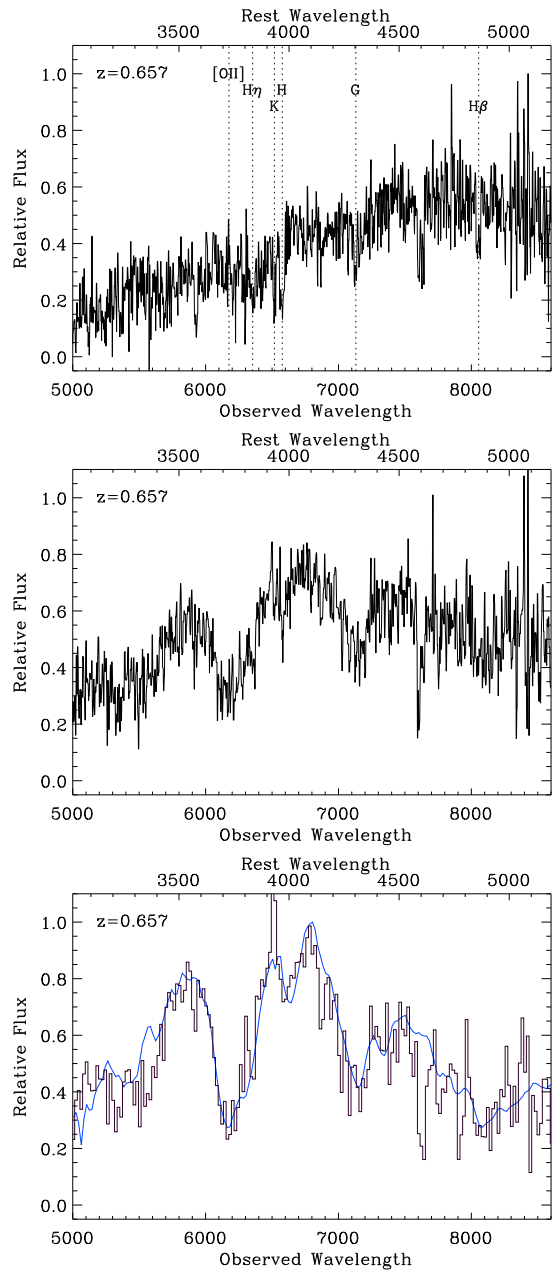


Fig. 8.— (Upper) Lightly smoothed spectrum of the host (or possible neighbour) galaxy of SN 1997R (atmospheric absorption has not been corrected in this spectrum). (Middle) Lightly smoothed spectrum of SN 1997R. (Lower) Rebinning spectrum of SN 1997R (histogram) after interpolating over narrow host galaxy lines, rebinning to 20 Å and subtracting template Sa galaxy, compared with SN 1989B at -5 days (smooth curve).

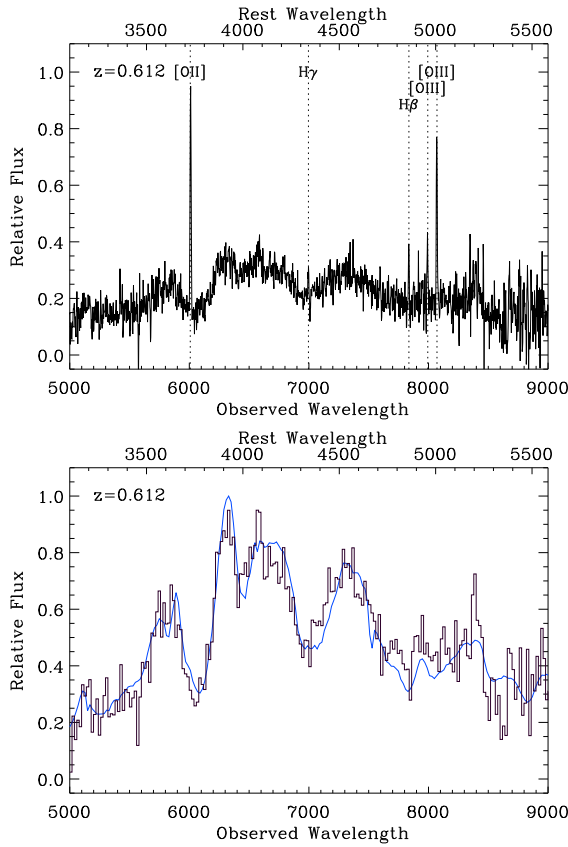


Fig. 9.— (Upper) Unsmoothed spectrum of SN 1997S showing the narrow lines used to determine the redshift. (Lower) rebinned spectrum of SN 1997S (histogram) after interpolating over strong emission lines of [OII] and [OIII], $H\beta$ and $H\gamma$ and subtraction of a SB1 host galaxy template, compared with SN 1992A at +5 days (smooth curve).

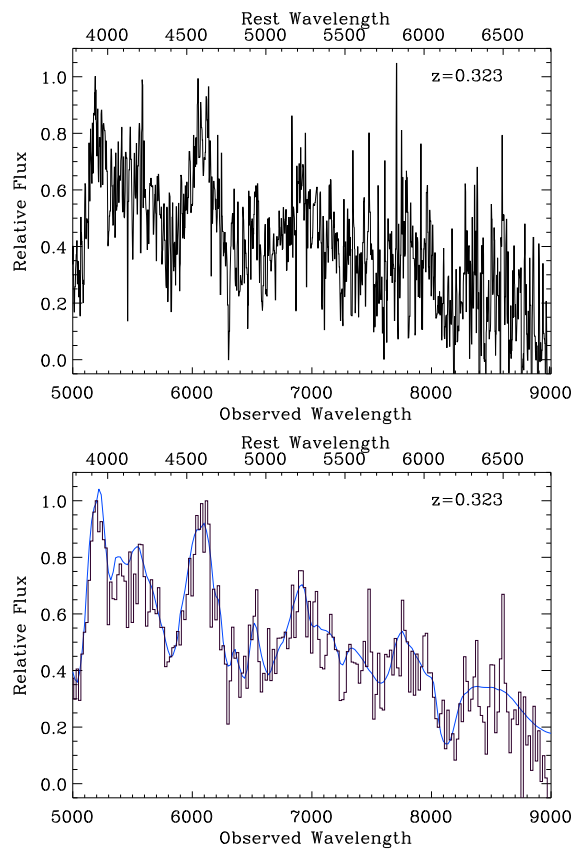


Fig. 10.— (Upper) lightly smoothed spectrum of SN 1997ac. (Lower) rebinned spectrum of SN 1997ac (histogram) compared with SN 1998bu at + 11 days (smooth curve).

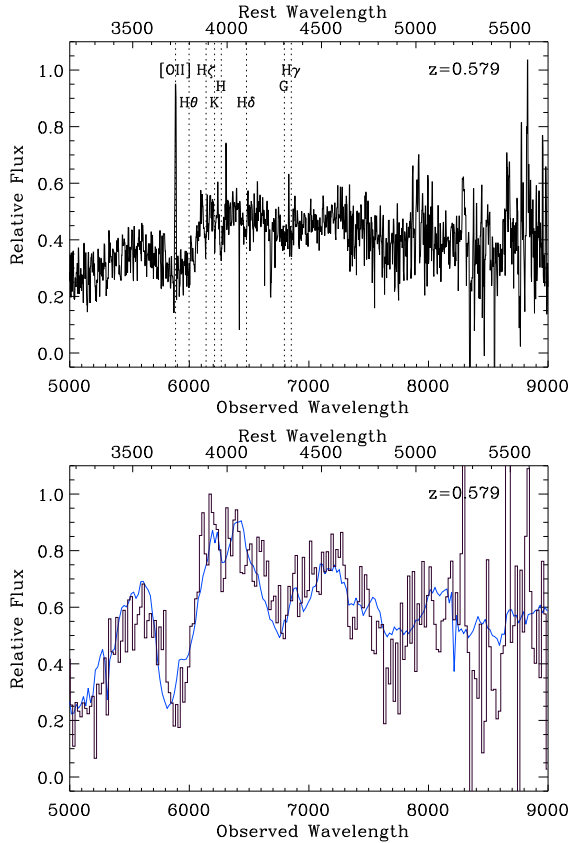


Fig. 11.— (Upper) Unsmoothed spectrum of the host of SN 1997af showing the narrow lines used to determine the redshift. (Lower) rebinned spectrum of SN 1997af (histogram) after interpolating across narrow lines from the host galaxy and subtracting an SB6 galaxy template, compared with the Type Ia SN 1999bp at -2 days (smooth curve).

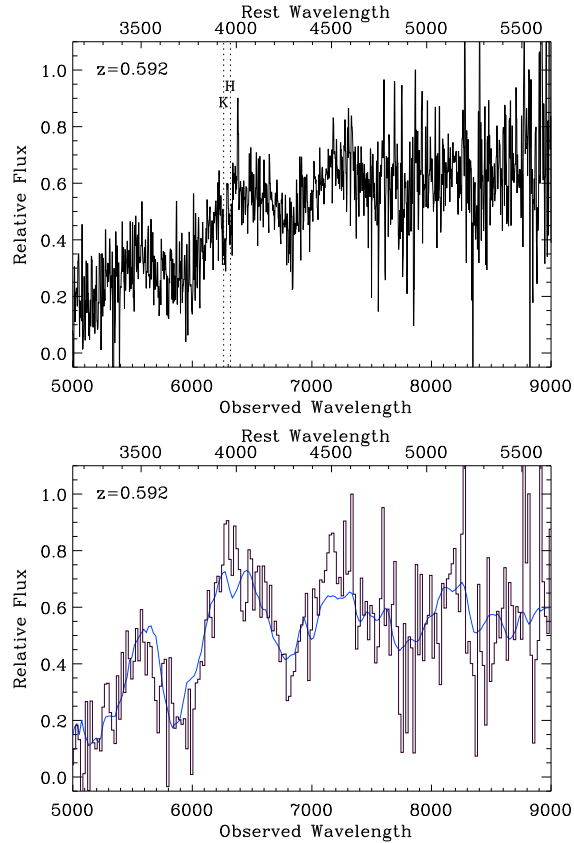


Fig. 12.— (Upper) Lightly smoothed spectrum of SN 1997ag showing narrow features used to determine the redshift. (Lower) rebinned spectrum SN 1997ag (histogram) after interpolating over narrow galaxy lines, compared with the Type Ia SN 1990N at $+7$ days before maximum (smooth curve).

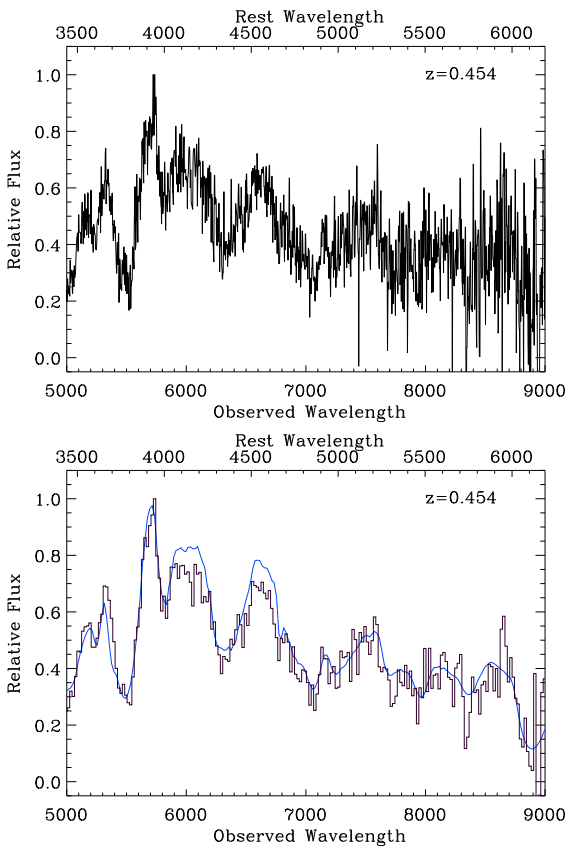


Fig. 13.— (Upper) Lightly smoothed spectrum of SN 1997ai. (Lower) rebinned spectrum of SN 1997ai (histogram) compared to the Type Ia SN 1992A at +5 days (smooth curve).

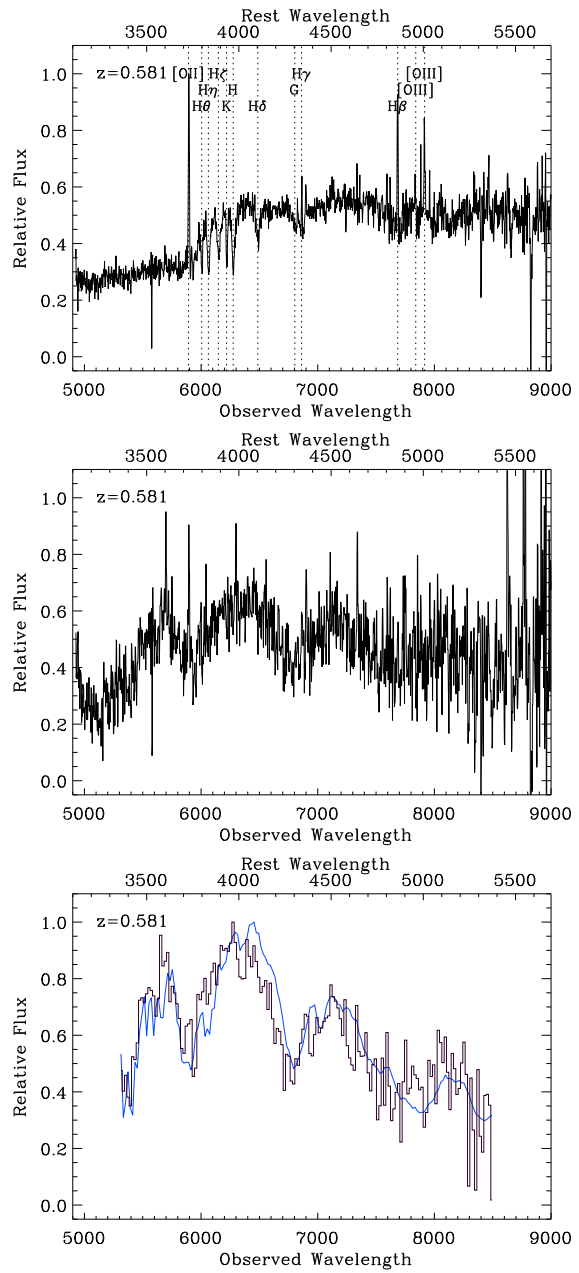


Fig. 14.— (Upper) Unsmoothed spectrum of the host of SN 1997aj (a separate extraction was possible although there are still narrow galaxy lines in the SN extraction) showing the narrow lines used to determine the redshift. (Middle) lightly smoothed spectrum of the supernova SN 1997aj. (Lower) Rebinne spectrum of SN 1997aj (histogram) after interpolating over narrow host galaxy lines of [OII] and Ca H&K and subtracting Sb galaxy light, compared with the Type Ia SN 1999aa at -3 days (smooth curve).

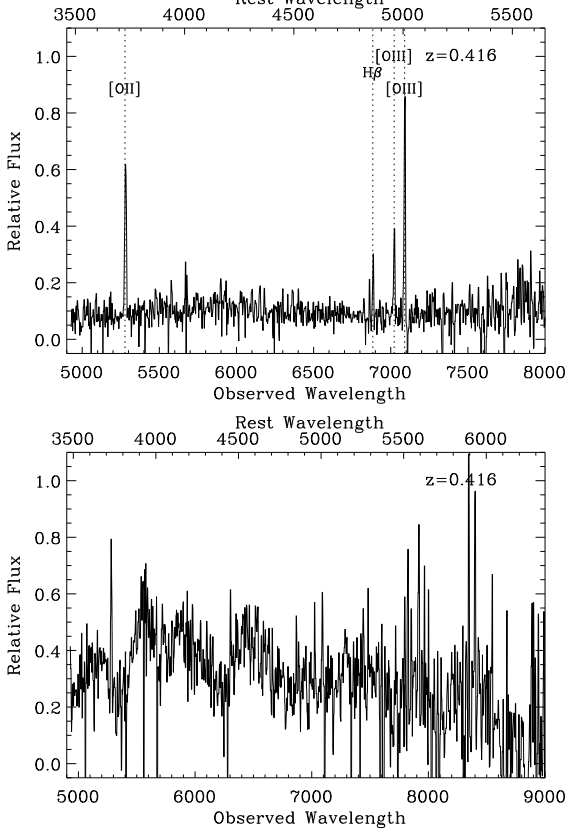


Fig. 15.— (Upper) Unsmoothed spectrum of the host of SN 1997am showing the narrow lines used to determine the redshift. (Lower) lightly smoothed spectrum of SN 1997am.

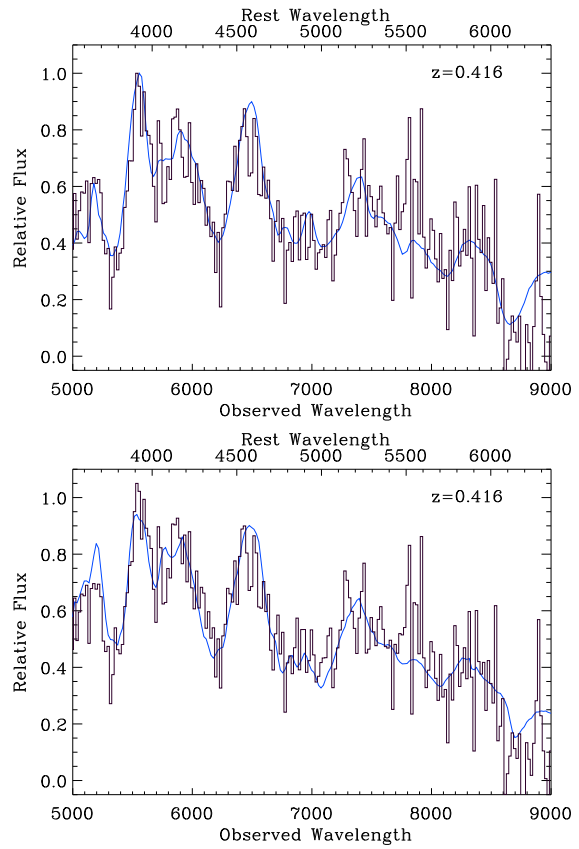


Fig. 15.— cont. (Upper) Rebinned spectrum of SN 1997am (histogram) after interpolating across cosmic rays and narrow lines from the host galaxy and subtraction of a SB1 galaxy template, compared with the Type Ia SN 1992A at +9 days (smooth curve). (Lower) previous plot but with the Type Ia SN 1991T at +10 days for comparison.

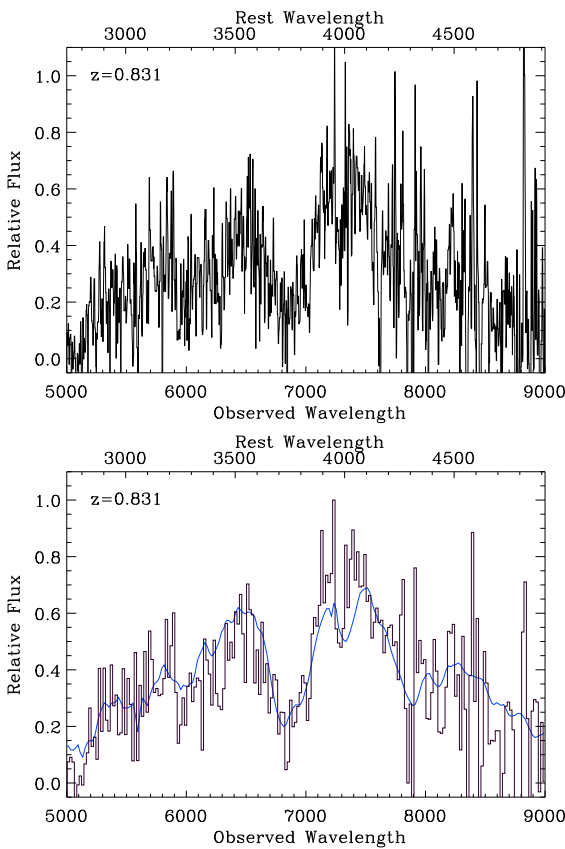


Fig. 16.— (Upper) Lightly smoothed spectrum of SN 1997ap. (Lower) Rebinned spectrum of SN 1997ap (histogram) after interpolating across the sky absorption region at 7600Å compared with the Type Ia SN 1989B at -5 days (smooth curve).

SN 1997I (Figure 5). The redshift of $z = 0.172 \pm 0.001$ was derived from galaxy lines ($\text{H}\alpha$, $\text{H}\beta$, SII, [OIII]). The spectrum is an excellent match to SN Ia features, including the 6150Å Si II feature seen at $\lambda_{\text{obs}} \sim 7200\text{\AA}$ and SII. The identification of this SN as a Type Ia is unambiguous, as the Si II and SII lines can easily be seen.

SN 1997J (Figure 6). Narrow absorption lines in the spectrum (Ca II H&K + 4000Å break from the host galaxy) give $z = 0.619 \pm 0.001$. SN Ia features at this redshift are clearly visible, despite being affected by the galaxy absorption lines. After subtracting a template S0 galaxy spectrum the features become much more clear. Here also, the Type Ia identification is most probable, but not definitive.

SN 1997N (Figure 7). The redshift of $z = 0.180 \pm 0.001$ was derived from narrow galaxy lines ($\text{H}\alpha$ [OIII] and possibly SII). SN Ia features from ~ 2 weeks after maximum are clearly visible in the spectrum including the Si II 6150Å feature seen at $\lambda_{\text{obs}} \sim 7250\text{\AA}$. The spectra of the low-redshift supernovae SN 1991T and SN 1994D both match this spectrum equally well (see section 7.2).

SN 1997R (Figure 8). The host (or a neighbouring) galaxy $2.6''$ away has $z = 0.657 \pm 0.001$ (identified from the Ca H&K lines and the 4000Å break). The supernova shows clear broad features matching a Type Ia at this redshift including the 4000Å Si II feature seen at $\lambda_{\text{obs}} \sim 6630\text{\AA}$, just redward of the Ca II feature. Narrow lines ($\text{H}\eta$, $\text{H}\delta$ and possibly $\text{H}\gamma$) are also visible in the spectrum, presumably from the host galaxy.

SN 1997S (Figure 9). Narrow lines due to the host galaxy ([OIII], [OII], $\text{H}\beta$, $\text{H}\gamma$) give $z = 0.612 \pm 0.001$. Very clear SN Ia features matching this redshift are visible including the Ca II, Si II(4000Å) and Fe II features.

SN 1997ac (Figure 10). The spectrum shows very clear SN Ia features at a redshift of $z = 0.323 \pm 0.005$ at ~ 10 days after maximum light. Since there are no clear features due to the host galaxy, the redshift is based solely on the supernova features. The Si 6150Å feature is clearly visi-

ble at an observed wavelength of $\sim 8100\text{\AA}$, providing an unambiguous identification of the object as a SN Ia.

SN 1997af (Figure 11). The supernova and host galaxy spectra could not be extracted separately. Narrow lines due to the host galaxy of [OII], Ca H&K, H γ , G-band, H η , H θ , are clear in the spectrum, giving a redshift of $z = 0.579 \pm 0.001$. The spectrum also shows broad features consistent with the spectrum of a SN Ia at the same redshift, including the small Si II feature (4000 \AA rest wavelength) at an observed wavelength of $\sim 6350\text{\AA}$.

SN 1997ag (Figure 12). The supernova and host light are blended and it was not possible to obtain separate extractions. The Ca H&K lines from the host galaxy are visible at $\lambda_{obs} = 6266\text{\AA}$ and 6317\AA giving a redshift of $z = 0.592 \pm 0.001$. SN Ia features are clearly visible in the spectrum, especially broad Ca II and Fe II.

SN 1997ai (Figure 13). The spectrum shows very clear SN Ia features at a redshift of $z = 0.454 \pm 0.006$. Since there are no clear features due to the host galaxy, the redshift is based solely on the supernova features. The lack of host galaxy contamination is confirmed by the fitting program, which used no galaxy light in its fit of the spectrum. The Si II (6150 \AA) feature is clearly visible at an observed wavelength of $\sim 8900\text{\AA}$, providing an unambiguous identification of the object as SN Ia.

SN 1997aj (Figure 14). The supernova and host were separated by $2.5''$ on the slit and their spectra could be extracted separately. The host galaxy spectrum shows emission lines of [OII], [OIII] and H β as well as absorption lines of H γ , H δ , H θ , H η , G-band and Ca H& K, at a redshift of $z = 0.581 \pm 0.001$. The supernova spectrum is consistent with that of a Type Ia at $z = 0.581$ showing the a strong, broad Fe II 5000 \AA feature seen at $\lambda_{obs} \sim 7900\text{\AA}$, but a relatively narrow Ca II 3800 \AA feature seen at $\lambda_{obs} \sim 6000\text{\AA}$.

SN 1997am (Figure 15). Separate extractions of the host galaxy and supernova were possible since they were separated by $2.3''$ on the slit. The

host galaxy spectrum shows emission lines of [OII], H β and [OIII] at a redshift of $z = 0.416 \pm 0.001$. The supernova spectrum is a good match to the normal Type Ia SN 1992A spectrum at day +9 and clearly shows the presence of the Si II (6150 \AA) feature seen at $\lambda_{obs} \sim 8710\text{\AA}$. SN 1991T at day +10 is also a good fit to the spectrum (see Section 7.2).

SN 1997ap (Figure 16). The redshift of $z = 0.831 \pm 0.007$ is based on supernova features alone. This spectrum was discussed in detail in Perlmutter et al. (1998). The slightly improved redshift estimate presented here superceeds that of earlier papers (Perlmutter et al. 1998, 1999; Knop et al. 2003). We note here that it was identified as a SN Ia by the presence of both the blue Ca II and Si II features.

7. Tests for Evolution

Although these spectra were taken primarily for the purposes of redshift measurement and SN classification, they also allow some basic tests of supernova evolution with redshift. We show that SNe Ia do not look dramatically different at high redshift, that they have similar elemental velocities, and that SNe Ia fall into the same sub-classes at high redshift.

7.1. Spectral morphology

High-redshift SNe Ia look similar to their low-redshift counterparts, but the implications for constraints on evolution are complicated. Figure 17 shows a selection of the high-redshift spectra (those not significantly contaminated by host galaxy light) plotted in order of rest frame days past maximum. These are interspersed with the time sequence for the nearby Branch-normal Type Ia supernova SN 1992A. Note that because the high-redshift spectra are not spectrophotometric measurements (see sections 3 and 5.2), differences in overall slope of the spectra should not be considered significant. Despite the lower S/N of the high-redshift spectra, and the non-uniform wavelength coverage (since the spectra have been de-redshifted by different amounts) it is clear that the overall trends in the spectral evolution with light curve phase are the same at low and high redshift. Furthermore, Figures 3 to 16 show that

high-redshift SNe resemble well observed local SNe on an object-by-object basis.

7.2. The incidence of spectroscopically peculiar SNe

Li et al. (2001a,b) make the case that, while slow-declining, spectroscopically peculiar SNe like SN 1991T and SN 1999aa represent 20% of SNe discovered in volume-limited local surveys, they are strangely absent from high-redshift SN samples. This is paradoxical, since these SNe are over-luminous, and so should be seen in *greater* numbers in flux-limited surveys. The authors present one possible solution — that these SNe become spectroscopically normal with time, and they appear normal by the time spectra are taken.

Perhaps supporting this idea, for two of our cases, both taken at relatively late times after maximum light, the spectrum of SN 1991T fits as well as the spectrum of a more normal supernova. SN 1997am has a light curve stretch (a measure of the rise and decline time of the supernova light curve, defined in Perlmutter et al. (1999)) of $s = 1.03 \pm 0.06$ (Knop et al. 2003), which is consistent with the stretch of SN 1991T ($s = 1.08$). Since the spectrum was taken approximately 10 rest-frame days after maximum light, by which time SN 1991T itself appears to be fairly spectroscopically normal, there is no definitive spectroscopic evidence that SN 1997am is a peculiar Type Ia, but it cannot be ruled out. In the other case, SN 1997N, the spectrum was taken approximately 16 rest-frame days after maximum. It is possible that this SN looked spectroscopically similar to SN 1991T at early times although again there is no definitive spectroscopic evidence for this. The stretch of SN 1997N is $s = 1.03 \pm 0.02$, somewhat lower than that of SN 1991T. However we note that the nearby SN 1997br also resembled SN 1991T spectroscopically, yet had a fairly normal light curve, with $\Delta m_{15}(B) = 1.00 \pm 0.15$, $s = 1.04$ (Li et al. 1999). Garavini et al. (in preparation) have found definitive evidence for a SN 1991T-like supernova at high redshift. In that case the spectrum was taken 7 days before maximum when the spectral peculiarities are more evident.

The explanation for the supposed dearth of SN 1991T-like SNe at high redshift proposed by Li et al. (that they are in the data set, but appear spectroscopically normal when spectra are taken)

appears to be part of the answer to the paradox, although the situation may be more complicated. These SNe may not be as consistently over-luminous as first thought (Li et al. 1999; Saha et al. 2001; Gibson & Stetson 2001), thus Li et al. (2001a) may have over-predicted the expected numbers in a flux-limited survey.

At the other extreme, spectroscopically peculiar under-luminous SNe like SN 1991bg (Filippenko et al. 1992; Leibundgut et al. 1993; Turatto et al. 1996) and SN 1999by (Toth & Szabó 2000; Howell et al. 2001; Vinkó et al. 2001; Höflich et al. 2002) have not been seen at high redshift. While it is unlikely that these SNe will be found in flux-limited searches, it is also possible that these SNe are from such an old stellar population that they do not exist at $z > 0.5$ (Howell 2001).

7.3. Calcium velocities

While the depth of absorption lines gives some information about the quantity of an ion in a SN, the velocity of the line gives information about the ion's distribution within the photosphere. Furthermore, the velocity of the supernova ejecta is related to the overall kinetic energy of the event. The kinetic energy has a direct influence on the opacities and hence on the total brightness of the supernova and its light-curve shape.

In Figure 18 we present a plot of the velocities of the Ca II minima for the SCP high-redshift supernovae compared with two well-observed nearby supernovae. We note that while the absorption feature at 3700Å is dominated by Ca II, Si II and various ionization states of the iron-peak elements (see Hatano et al. 1999) also contribute. For the three lowest redshift supernovae in the SCP set, the Ca II feature is outside the observed wavelength range. Therefore this analysis is restricted to the SCP supernovae with $z > 0.38$.

The analysis was performed on the spectra after galaxy subtraction had been done if this was necessary (as described in the previous section). The Ca II velocities were estimated by fitting a Gaussian function to the region 3610Å to 3870Å in the rest frame, followed by a second iteration using the region from -65Å to +100Å either side of the previous estimate of the minimum. The velocity shift was calculated from the wavelength of the minimum by assuming a rest frame wavelength

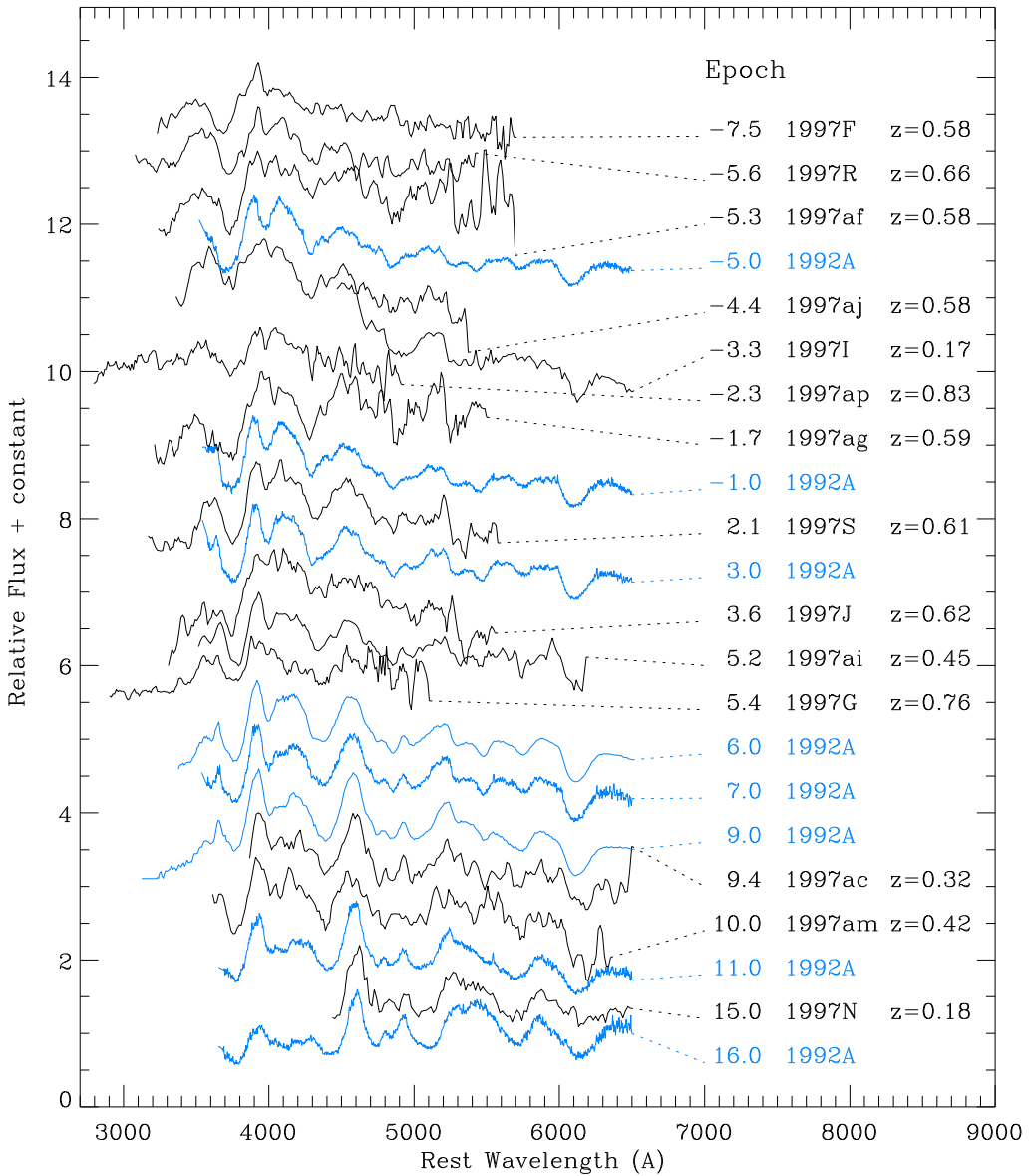


Fig. 17.— The time sequence of high redshift supernova spectra in order of rest-frame date relative to maximum light, as determined from the light curve (τ_{lc}). Spectra of the nearby Type Ia, SN 1992A are interspersed for comparison.

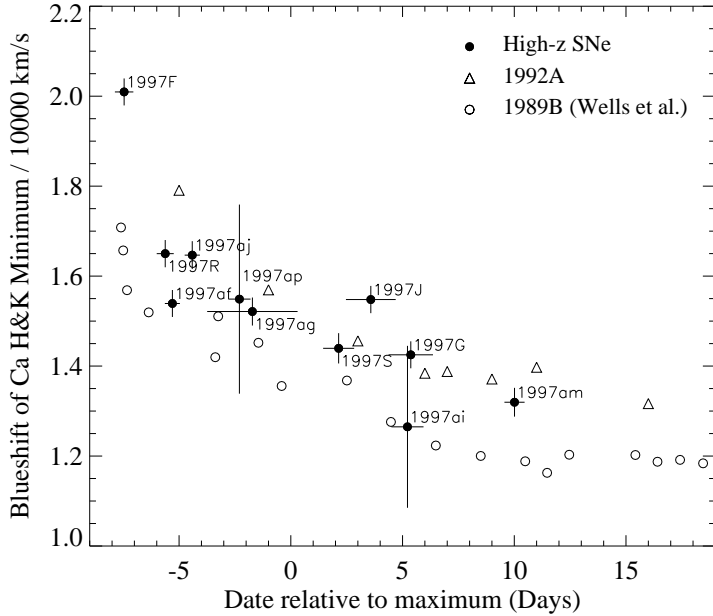


Fig. 18.— Comparison of the velocities determined for the minima of the Ca II feature for two well observed nearby SNe Ia (1992A and 1989B) and the high-redshift SNe presented in this paper.

for this feature of 3945.28\AA . The same analysis was done on a spectral series for the normal Type Ia SN1992A (Kirshner et al. 1993). Finally the published Ca II velocities for the normal Type Ia supernova 1989B (Wells et al. 1994) are also shown.

The general trend of decreasing Ca II velocities as a function of time and the range in velocities at a given epoch seen in the data is completely consistent with the range seen in nearby observations. This result is confirmed by Garavini et al. (in preparation) in a more recent independent set of high-redshift SN spectra.

Our high-redshift data is also broadly consistent with the recent study of nearby SNe by Benetti et al. (2005), although the comparison is complicated by the fact that Benetti et al. measure Si II velocities whereas we consider Ca II velocities. Taking into account the apparent offset between the two (as can be seen from SN 1992A and SN 1989B for example), the velocities seen in our high-redshift sample (including the large value for SN 1997F) are broadly consistent with the range of velocities seen in nearby SNe. Because of the larger error bars at high redshift, and

only having a single velocity measurement per SN, it is not possible to determine into which of the Benetti et al. (2005) classes each of our objects would fall.

8. Conclusions

At the present time, the statistical and systematic errors in the measurement of the cosmological parameters from Type Ia supernovae are of similar size. As the quality and quantity of high-redshift supernova observations grows it will become even more important to constrain the systematic uncertainties. Non-Ia contamination and evolution are two of the larger potential systematics we currently face. Here we have presented some of the methods we employ to reduce/study these uncertainties.

In this paper we have presented spectra for 14 high-redshift supernovae and demonstrated that the spectra are consistent with Type Ia. In three cases at intermediate redshift (SN 1997ac, SN 1997ai and SN 1997am at $z \sim 0.3 - 0.5$) in addition to two at lower redshift (SN 1997I and SN 1997N) we have observed the Si II 6150\AA fea-

ture and hence have unambiguously identified the SN as Type Ia. For higher redshifts this Si II feature becomes increasingly difficult to observe as fringing and poor CCD response in the red, and bright OH lines in the sky background makes the spectra very noisy redward of $\sim 9500\text{\AA}$. Here we have used spectral matching combined with the identification of specific spectral features to identify the objects as SN Ia, the most important being the identification of Si II features near 4000\AA .

We have carried out first-order quantitative tests to compare the high-redshift spectra with their low-redshift counterparts.

We show that the spectral phase determined from spectral matching to low-redshift Type Ia spectra is in very good agreement with the phase determined from the high-redshift light curve. Similarly the spectral time series shows the same overall trends at low and high redshift. Finally, quantitative measurements of the Calcium ejection velocity in the high-redshift spectra are also consistent with those measured from the spectra of low-redshift Branch-normal Type Ia SNe. Therefore we have found no evidence for evolution in the population of Type Ia SNe up to redshifts of $z \sim 0.8$. While we cannot prove that all SNe Ia at high redshift are identical to their low-redshift counterparts, we can say that it is possible to choose a set of high-redshift SNe Ia that are equivalent to low-redshift counterparts to within the accuracy of these quantitative tests.

With larger samples, such as those now being collected by the Supernova Legacy Survey (SNLS, Pritchett (2005)) and the ESSENCE project (Matheson et al. (2005) and references therein) it will be possible to make more detailed comparisons in smaller redshift bins in the range $0.2 < z < 1$ and in subsets based on light curve stretch, galaxy host type and other factors. Such studies will provide further confidence in the use of SNe Ia as distance indicators, and, in cases where quantitative measurements of spectral features are found to correlate with luminosity or light curve stretch (e.g. Nugent et al. 1995; Folatelli 2004), these can be used to reduce scatter in the Hubble diagram and thus improve the precision to which cosmological parameters may be measured.

Acknowledgements

The authors acknowledge the help of the night assistants and support staff at the telescopes from which data for this paper were obtained.

We thank the anonymous referee for a very thorough reading of the paper and helpful suggestions.

This paper makes use of light curve photometry collected at the Cerro Tololo Inter-American Observatory, which is operated by Association of Universities for Research in Astronomy, Inc. under a cooperative agreement with the National Science Foundation. Based in part on observations obtained at the WIYN Observatory, which is a joint facility of the University of Wisconsin-Madison, Indiana University, Yale University, and the National Optical Astronomy Observatory. We also make use of observations made with the NASA/ESA Hubble Space Telescope, obtained at the Space Telescope Science Institute, which is operated by the Association of Universities for Research in Astronomy, Inc., under NASA contract NAS 5-26555. These observations are associated with programs DD-7590 and GO-7336.

This work was supported in part by the Royal Swedish Academy of Sciences and by the Director, Office of Science, Office of High Energy and Nuclear Physics, of the US Department of Energy under Contract No. DE-AC03-76SF00098. Support for this work was provided by NASA through grant HST-GO-7336 from the Space Telescope Science Institute, which is operated by the Association of Universities for Research in Astronomy, Inc., under NASA contract NAS 5-26555.

REFERENCES

- Baldwin, J. A., & Stone, R. P. S. 1984, MNRAS, 206, 241
- Barris, B. J., Tonry, J., Blondin, S., Challis, P., Chornock, R., Clocchiatti, A., Filippenko, A. V., Garnavich, P., Holland, S. T., Jha, S., Kirshner, R. P., Krisciunas, K., Leibundgut, B., Li, W., Matheson, T., Miknaitis, G., Phillips, M. M., Riess, A. G., Schmidt, B., Smith, R. C., Sollerman, J., Spyromilio, J., Stubbs, C. W., Suntzeff, N. B., Aussel, H., Chambers, K. C., Connelly, M. S., D., D., Henry, J., Kaiser, N.,

- Liu, M., Martin, E., & Wainscoat, R. J. 2004, ApJ, 602, 571
- Benetti, S., Cappellaro, E., Mazzali, P. A., Turatto, M., Altavilla, G., Bufano, F., Elias-Rosa, N., Kotak, R., Pignata, G., Salvo, M., & Stanishev, V. 2005, ApJ, 623, 1101
- Buzzoni, B., Delabre, B., Dekker, H., Dodorico, S., Enard, D., Focardi, P., Gustafsson, B., Nees, W., Paureau, J., & Reiss, R. 2004, ESO Messenger
- Cappellaro, E., Turatto, M., & Fernley, J. 1995, IUE-ULDA Access Guide No. 6: Supernovae (ESA SCIENTIFIC PUBLICATION ESA-SP 1189)
- Cardelli, J. A., Clayton, G. C., & Mathis, J. S. 1989, ApJ, 345, 245
- Clocchiatti, A., Wheeler, J. C., Brotherton, M. S., Cochran, A. L., Wills, D., Barker, E. S., & Turatto, M. 1996, ApJ, 462, 462
- Coil, A. L., Matheson, T., Filippenko, A. V., Leonard, D. C., Tonry, J., Riess, A. G., Challis, P., Clocchiatti, A., Garnavich, P. M., Hogan, C. J., Jha, S., Kirshner, R. P., Leibundgut, B., Phillips, M. M., Schmidt, B. P., Schommer, R. A., Smith, R. C., Soderberg, A. M., Spyromilio, J., Stubbs, C., Suntzeff, N. B., & Woudt, P. 2000, ApJ, 544, L111
- Filippenko, A. V. 1997, ARA&A, 35, 309
- Filippenko, A. V., Richmond, M. W., Branch, D., Gaskell, M., Herbst, W., Ford, C. H., Treffers, R. R., Matheson, T., Ho, L. C., Dey, A., Sargent, W. L. W., Small, T. A., & van Breugel, W. J. M. 1992, AJ, 104, 1543
- Folatelli, G. 2004, Ph.D. thesis, Stockholm University
- Garnavich, P., et al. 1998, ApJ, 509, 74
- Gibson, B. K., & Stetson, P. B. 2001, ApJ, 547, L103
- Höflich, P., Gerardy, C. L., Fesen, R. A., & Sakai, S. 2002, ApJ, 568, 791
- Hamuy, M. 1994, PASP, 106, 566
- Hatano, K., Branch, D., Fisher, A., Millard, J., & Baron, E. 1999, ApJS, 121, 233
- Howell, D. A. 2001, ApJ, 554, L193
- Howell, D. A., Höflich, P., Wang, L., & Wheeler, J. C. 2001, ApJ, 556, 302
- Howell, D. A., & Wang, L. 2002, American Astronomical Society Meeting, 201, 0
- Kinney, A. L., Bohlin, R. C., Calzetti, D., Panagia, N., & Wyse, R. F. G. 1993, ApJS, 86, 5
- Kirshner, R., et al. 1993, ApJ, 415, 589
- Knop, R., Aldering, G., Amanullah, R., Astier, P., Blanc, G., Burns, M. S., Conley, A., Deustua, S. E., Doi, M., Fabbro, S., Folatelli, G., Fruchter, A. S., Garavini, G., Gibbons, R., Goldhaber, G., Goobar, A., Groom, D. E., Hardin, D., Hook, I., Howell, D. A., Irwin, M., Kim, A. G., Knop, R. A., Lidman, C., McMahon, R., Mendez, J., Nobili, S., Nugent, P. E., Pain, R., Panagia, N., Pennypacker, C. R., Perlmutter, S., Quimby, R., Raux, J., Regnault, N., Ruiz-Lapuente, P., Schaefer, B., Schahmaneche, K., Spadafora, A. L., Walton, N. A., Wang, L., Wood-Vasey, W. M., & Yasuda, N. 2003, ApJ, 598, 102
- Leibundgut, B., Kirshner, R. P., Phillips, M. M., Wells, L. A., Suntzeff, N. B., Hamuy, M., Schommer, R. A., Walker, A. R., Gonzalez, L., Ugarte, P., Williams, R. E., Williger, G., Gomez, M., Marzke, R., Schmidt, B. P., Whitney, B., Coldwell, N., Peters, J., Chaffee, F. H., Foltz, C. B., Rehner, D., Siciliano, L., Barnes, T. G., Cheng, K.-P., Hintzen, P. M. N., Kim, Y.-C., Maza, J., Parker, J. W., Porter, A. C., Schmidtke, P. C., & Sonneborn, G. 1993, AJ, 105, 301
- Li, W., Filippenko, A. V., & Riess, A. G. 2001a, ApJ, 546, 719
- Li, W., Filippenko, A. V., Treffers, R. R., Riess, A. G., Hu, J., & Qiu, Y. 2001b, ApJ, 546, 734
- Li, W. D., Qiu, Y. L., Qiao, Q. Y., Zhu, X. H., Hu, J. Y., Richmond, M. W., Filippenko, A. V., Treffers, R. R., Peng, C. Y., & Leonard, D. C. 1999, AJ, 117, 2709
- Lidman, C., et al. 2005, A&A, 430, 843

- Matheson, T., et al. 2005, AJ, 129, 2352
- Meikle, W. P. S., Cumming, R. J., Geballe, T. R., Lewis, J. R., Walton, N. A., Balcells, M., Cimatti, A., Croom, S. M., Dhillon, V. S., Economou, F., Jenkins, C. R., Knapen, J. H., Meadows, V. S., Morris, P. W., Perez-Fournon, I., Shanks, T., Smith, L. J., Tanvir, N. R., Veilleux, S., Vilchez, J., Wall, J. V., & Lucey, J. R. 1996, MNRAS, 281, 263
- Nugent, P., Phillips, M., Baron, E., Branch, D., & Hauschildt, P. 1995, ApJ, 455, L147
- O'Donnell, J. E. 1994, ApJ, 422, 158
- Oke, J., Cohen, J., Carr, M., Cromer, J., Dinzizian, A., Harris, F., Labrecque, S., Lucinio, R., Schaal, W., Epps, H., & Miller, J. 1995, PASP, 375
- Oke, J. B., & Gunn, J. E. 1983, ApJ, 266, 713
- Perlmutter, S., Pennypacker, C. R., Goldhaber, G., Goobar, A., Muller, R. A., Newberg, H. J. M., Desai, J., Kim, A. G., Kim, M. Y., Small, I. A., Boyle, B. J., Crawford, C. S., McMahon, R. G., Bunclark, P. S., Carter, D., Irwin, M. J., Terlevich, R. J., Ellis, R. S., Glazebrook, K., Couch, W. J., Mould, J. R., Small, T. A., & Abraham, R. G. 1995, ApJ, 440, L41
- Perlmutter, S., et al. 1997, in Thermonuclear Supernova, edited by P. Ruiz-Lapuente, R. Canal, & J. Isern (Dordrecht: Kluwer), 749
- 1998, Nature, 391
- 1999, ApJ, 517, 565
- Pritchett, C. 2005, in Observing Dark Energy, edited by S. Wolff, & T. Lauer (Provo: BYU Press)
- Richardson, D., Thomas, R., Casebeer, D., Branch, D., & Baron, E. 2002, American Astronomical Society, 201st AAS Meeting, #56.09; Bulletin of the American Astronomical Society, 34, 1205
- Riess, A., et al. 1998, AJ, 116, 1009
- Riess, A. G., Strolger, L.-G., Tonry, J., Casertano, S., Ferguson, H. C., Mobasher, B., Chalis, P., Filippenko, S., A. V. and Jha, Li, W., Chornock, R., Kirshner, R. P., Leibundgut, B., Dickinson, M., Livio, M., Giavalisco, M., Steidel, C. C., Benites, T., & Tsvetanov, Z. 2004, apj, 607, 665
- Saha, A., Sandage, A., Thim, F., Labhardt, L., Tammann, G. A., Christensen, J., Panagia, N., & Macchietto, F. D. 2001, ApJ, 551, 973
- Schmidt, B. P., Suntzeff, N. B., Phillips, M. M., Schommer, R. A., Clocchiatti, A., Kirshner, R. P., Garnavich, P., Challis, P., Leibundgut, B., Spyromilio, J., Riess, A. G., Filippenko, A. V., Hamuy, M., Smith, R. C., Hogan, C., Stubbs, C., Diercks, A., Reiss, D., Gilliland, R., Tonry, J., Maza, J., Dressler, A., Walsh, J., & Ciardullo, R. 1998, ApJ, 507, 46
- Stone, R. P. S., & Baldwin, J. A. 1983, MNRAS, 204, 347
- Sullivan, M., Ellis, R. S., Aldering, G., Amanullah, R., Astier, P., Blanc, G., Burns, M. S., Conley, A., Deustua, S. E., Doi, M., Fabbro, S., Folatelli, G., Fruchter, A. S., Garavini, G., Gibbons, R., Goldhaber, G., Goobar, A., Groom, D. E., Hardin, D., Hook, I., Howell, D. A., Irwin, M., Kim, A. G., Knop, R. A., Lidman, C., McMahon, R., Mendez, J., Nobili, S., Nugent, P. E., Pain, R., Panagia, N., Pennypacker, C. R., Perlmutter, S., Quimby, R., Raux, J., Regnault, N., Ruiz-Lapuente, P., Schaefer, B., Schahmaneche, K., Spadafora, A. L., Walton, N. A., Wang, L., Wood-Vasey, W. M., & Yasuda, N. 2003, MNRAS, 340, 1057
- Tonry, J. L., Schmidt, B. P., Barris, B., Candia, P., Challis, P., Clocchiatti, A., Coil, A. L., Filippenko, A. V., Garnavich, P., Hogan, C., Holland, S. T., Jha, S., Kirshner, R. P., Krisciunas, K., Leibundgut, B., Li, W., Matheson, T., Phillips, M. M., Riess, A. G., Schommer, R., Smith, R. C., Sollerman, J., Spyromilio, J., Stubbs, C. W., & Suntzeff, N. B. 2003, apj, 594, 1
- Toth, I., & Szabó, R. 2000, A&A, 361, 63
- Turatto, M., Benetti, S., Cappellaro, E., Danziger, I. J., della Valle, M., Gouiffes, C., Mazzali, P. A., & Patat, F. 1996, MNRAS, 283, 1

Vinkó, J., Kiss, L. L., Csák, B., Fűrész, G., Szabó, R., Thomson, J. R., & Mochnacki, S. W. 2001, AJ, 121, 3127

Wells, L. A., Phillips, M. M., Suntzeff, B., Heathcote, S. R., Hamuy, M., Navarrete, M., Fernandez, M., Weller, W. G., Schommer, R. A., Kirshner, R. P., Leibundgut, B., Willner, S. P., Peletier, S. P., Schlegel, E. M., Wheeler, J. C., Harkness, R. P., Bell, D. J., Matthews, J. M., Filippenko, A. V., Shields, J. C., Richmond, M. W., Jewitt, D., Luu, J., Tran, H. D., Appleton, P. N., Robson, E. I., Tyson, J. A., Guhathakurta, P., Eder, J. A., Bond, H. E., Potter, M., Veilleux, S., Porter, A. C., Humphreys, R. M., Janes, K. A., Williams, T. B., Costa, E., Ruiz, M. T., Lee, J. T., Lutz, J. H., Rich, R. M., Winkler, P. F., & Tyson, N. D. 1994, AJ, 108, 2233

Wells, L. A., et al. 1994, AJ, 108, 2233